Simplified Approach for Assessment of Low-Thrust Elliptical Orbit Transfers

James E. Pollard
The Aerospace Corporation, P.O. Box 92957, M5-754, Los Angeles, CA 90009

Abstract

Low-thrust elliptical orbit transfer missions are modeled by calculating the long-term variation of the orbital elements. Rate equations are given for perigee- and apogee-centered burn arcs with four different steering programs. Applications include varying the eccentricity at constant semimajor axis, transferring from low-earth orbit to a Molniya orbit, and transferring to geosynchronous orbit with an inclination change.

Introduction

Techniques for evaluating low-thrust orbit transfers are of current interest because electric thrusters will soon be used in missions with significant ΔV such as geosynchronous orbit insertion.[1-5] Exact numerical methods to describe low-thrust trajectories are computationally intensive and may be more elaborate than is needed for the first phase of a trade study. Moreover, designing a trajectory to minimize trip time or propellant mass could prove to be impractical, because the satellite may not be able to execute the optimal steering program envisioned for electric orbit transfer vehicles.[1] This paper presents an approach for estimating the ΔV and trip time in elliptical orbit transfers by calculating the long-term (secular) variation of the classical orbital elements using simple steering programs. The method permits a rapid assessment of design options for delivering a satellite to its final orbit, prior to a full optimization when the trade-space has been narrowed sufficiently.

Analysis

A useful formulation of the low-thrust orbit adjustment problem was developed by Burt[6] under the assumption that thrusting produces a negligible change in each element during a single period of the orbit. Hence the secular rate of change of one element can be calculated by holding the other elements constant during one revolution. We extend Burt's approach to the case of discontinuous acceleration by analyzing perigee- and apogee-centered burn arcs that can be used to transfer from low-earth to Molniya orbit or to raise the perigee of an elliptical orbit to geosynchronous orbit.[7] We solve for the secular rates of change of the elements using a specified steering program, and then integrate numerically to obtain the history of each element throughout the maneuver.

In Burt's nomenclature f is the thrust per unit mass (i.e., acceleration) having the three components

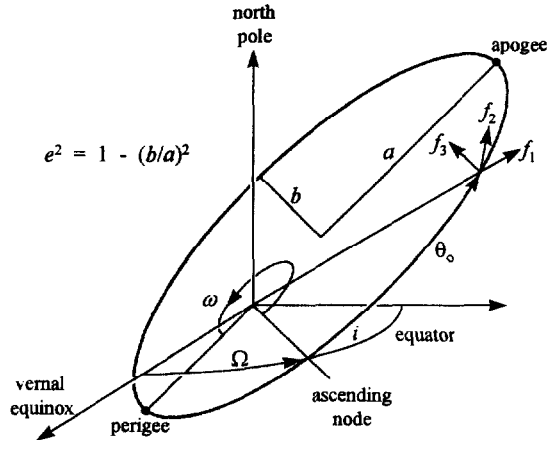

Figure 1. Orbital elements and components of acceleration in geocentric inertial coordinates.

shown in Fig. 1. Here, f_1 is directed outward along the radius vector, f_2 is normal to the radius vector in the orbit plane, and f_3 is normal to the orbit plane in the direction of the angular momentum vector. Table 1 gives the rates of change of the semimajor axis a, eccentricity e, inclination i, right ascension of the ascending node Ω, and argument of perigee ω as functions of eccentric anomaly E. These expressions are derived from the Lagrange planetary equations listed in Reference 6. We observe in Table 1 that a and e are affected by the in-plane components f_1 and f_2, that i and Ω are affected by the out-of-plane component f_3, and that ω is affected by all three components.

The magnitude of the acceleration $f = \sqrt{(f_1)^2 + (f_2)^2 + (f_3)^2}$ is taken to be constant throughout the mission. Specifying f_1, f_2, and f_3 as functions of E defines the steering program and determines the relative rates of change of the orbital elements. Table 2 lists $f_1(E)$ and $f_2(E)$ in four different pitch steering cases, where the in-plane acceleration vector is (1) perpendicular to the orbit radius vector, (2) tangent to the orbit path, (3) perpendicular to the major axis of the ellipse, and (4) parallel to the major axis of the ellipse. Cases (1) and (2) are identical in the limit of small e. We will treat examples in which the yaw steering angle β is fixed, meaning that the out-of-plane component of acceleration ($f_3 = f \sin \beta$) is constant during the mission. However, the formulas

Table 1. Rates of change of the orbital elements with E, where $\mu = 398{,}601$ km^3 s^{-2}.

$\frac{da}{dE}$	$\frac{2a^3}{\mu}\left(f_1 e \sin E + f_2\sqrt{1-e^2}\right)$
$\frac{de}{dE}$	$\frac{a^2}{\mu}\left[f_1\left(1-e^2\right)\sin E + f_2\sqrt{1-e^2}\left(2\cos E - e - e\cos^2 E\right)\right]$
$\frac{di}{dE}$	$\frac{a^2}{\mu} f_3\left(1-e\cos E\right)\left[\frac{(\cos E - e)\cos\omega}{\sqrt{1-e^2}} - \sin E \sin\omega\right]$
$\frac{d\Omega}{dE}$	$\frac{a^2}{\mu} f_3 \frac{1-e\cos E}{\sin i}\left[\frac{(\cos E - e)\sin\omega}{\sqrt{1-e^2}} + \sin E \cos\omega\right]$
$\frac{d\omega}{dE}$	$\frac{a^2}{\mu}\left\{\frac{1}{e}\left[-f_1\sqrt{1-e^2}\left(\cos E - e\right) + f_2\left(2-e^2-e\cos E\right)\sin E\right]\right.$ $\left. - f_3\left(1-e\cos E\right)\cot i\left[\frac{(\cos E - e)\sin\omega}{\sqrt{1-e^2}} + \sin E\cos\omega\right]\right\}$

presented below for the rates of change of the elements are also applicable to the case of a slowly varying yaw angle. Discontinuous thrusting is represented by perigee- or apogee-centered burns where the burn arc is either $-\alpha \le E \le +\alpha$ or $\pi - \alpha \le E \le \pi + \alpha$, as shown in Fig. 2. After inserting a steering program from Table 2 into the rate equations from Table 1, the resulting expressions are integrated over the burn arc to determine the change in each element during one revolution. Taking case (1) as an example, the change in the semimajor axis is

$$\Delta a = \int_{-\alpha}^{\alpha}\left(\frac{2a^3}{\mu} f_{12}\sqrt{1-e^2}\right)dE = \frac{4a^3}{\mu} f_{12}\sqrt{1-e^2}\;\alpha\,. \tag{1}$$

The secular rate of change of a is obtained by multiplying Δa times the orbit frequency, namely

$$\frac{d\overline{a}}{dt} = \frac{1}{2\pi}\sqrt{\frac{\mu}{a^3}}\left(\frac{4a^3}{\mu} f_{12}\sqrt{1-e^2}\;\alpha\right) = \frac{2 f_{12}}{\pi}\sqrt{\frac{a^3}{\mu}\left(1-e^2\right)}\,\alpha\,. \tag{2}$$

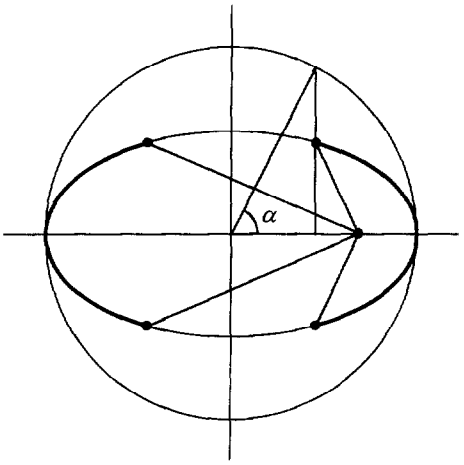

Figure 2. Perigee- and apogee-centered burn arcs are specified in units of eccentric anomaly E where $-\alpha \le E \le +\alpha$ or $\pi - \alpha \le E \le \pi + \alpha$.

Secular rates of change of a, e, i, Ω, and ω for the four steering programs are obtained by applying the above procedure to all of the elements, leading to the formulas in Table 3. Figure 3 compares secular rates for the different steering programs as a function of burn arc. When the burn arc is small the steering programs for cases (1), (2), and (3) become equivalent, and hence there is a convergence in the secular rates of change of a and e in the limit of small α as illustrated in Fig. 3. Case (2) steering is more efficient than case (1) for changing a by either apogee- or perigee-centered burns, while changing e is better performed by case (1) in apogee burns and by case (2) in perigee burns. Case (3) has the in-plane acceleration perpendicular to the major axis of the ellipse, which is rather ineffective for changing a, but for continuous thrusting ($\alpha = \pi$) it can

Table 2. In-plane (pitch) steering with four different choices for the in-plane acceleration vector, where $f_{12} \equiv \sqrt{(f_1)^2 + (f_2)^2} = f \cos\beta$.

	(1) Perpendicular to the orbit radius vector	(2) Tangent to the orbit path	(3) Perpendicular to the major axis of the ellipse	(4) Parallel to the major axis of the ellipse
$f_1(E)$	0	$\dfrac{f_{12}\, e \sin E}{\sqrt{1-e^2\cos^2 E}}$	$\dfrac{f_{12}\sqrt{1-e^2}\sin E}{1-e\cos E}$	$\dfrac{f_{12}(\cos E - e)}{1-e\cos E}$
$f_2(E)$	f_{12}	$f_{12}\sqrt{\dfrac{1-e^2}{1-e^2\cos^2 E}}$	$\dfrac{f_{12}(\cos E - e)}{1-e\cos E}$	$\dfrac{-f_{12}\sqrt{1-e^2}\sin E}{1-e\cos E}$

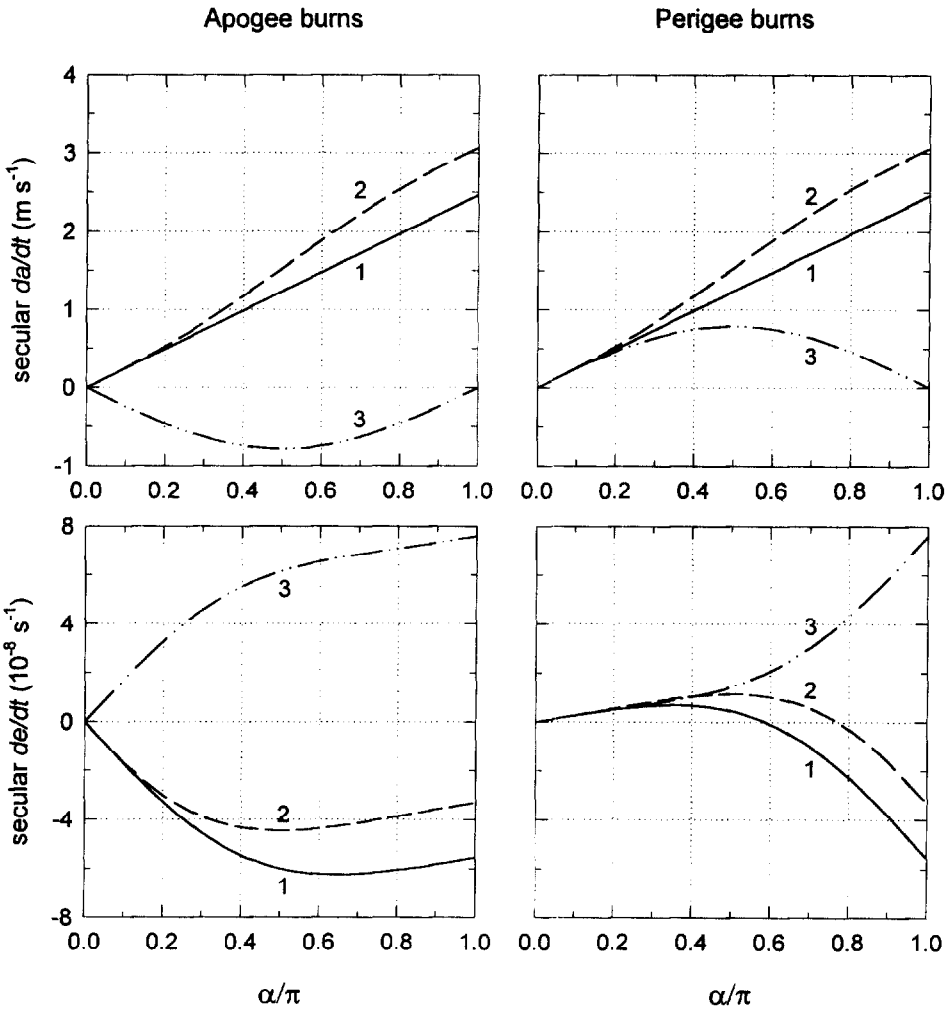

Figure 3. Comparison of in-plane steering cases (1), (2), and (3) in a GEO transfer orbit with an apogee altitude of 35,786 km and a perigee altitude of 185 km. Secular rates of change for a and e are calculated from Table 3 with $f = 3 \times 10^{-7}$ km/s^2, and with the burn arc given by α, as defined in Fig. 2.

Table 3. Secular rates of change of the orbital elements with four different choices for the in-plane acceleration vector.

	(1) Perpendicular to the orbit radius vector	(2) Tangent to the orbit path	(3) Perpendicular to the major axis of the ellipse	(4) Parallel to the major axis of the ellipse
$\frac{d\tilde{a}}{dt}$	$\frac{2 f_{12}}{\pi}\sqrt{\frac{a^3}{\mu}\left(1-e^2\right)}\,\alpha$	$\frac{2 f_{12}}{\pi}\sqrt{\frac{a^3}{\mu}}\int_0^{\alpha}\sqrt{1-e^2\cos^2 E}\;dE$	$\frac{-2\sigma f_{12}}{\pi}\sqrt{\frac{a^3}{\mu}\left(1-e^2\right)}\sin\alpha$	0
$\frac{d\tilde{e}}{dt}$	$\frac{-f_{12}}{2\pi}\sqrt{\frac{a}{\mu}\left(1-e^2\right)}\,(4\sigma\sin\alpha+3e\alpha + e\cos\alpha\sin\alpha)$	$\frac{2 f_{12}}{\pi}\sqrt{\frac{a}{\mu}\left(1-e^2\right)}H(\sigma,\alpha)$	$\frac{f_{12}}{2\pi}\sqrt{\frac{a}{\mu}\left(1-e^2\right)}\,(4\sigma\, e\sin\alpha + 3\alpha + \cos\alpha\sin\alpha)$	0
$\frac{d\tilde{i}}{dt}$	$\frac{-f_3}{2\pi}\sqrt{\frac{a}{\mu}}\cos\omega\;G(\sigma,\alpha,e)$	same as (1)	same as (1)	same as (1)
$\frac{d\tilde{\Omega}}{dt}$	$\frac{-f_3}{2\pi}\sqrt{\frac{a}{\mu}}\frac{\sin\omega}{\sin i}\,G(\sigma,\alpha,e)+N(a,e,i)$	same as (1)	same as (1)	same as (1)
$\frac{d\tilde{\omega}}{dt}$	$\frac{f_3}{2\pi}\sqrt{\frac{a}{\mu}}\cot i\sin\omega\;G(\sigma,\alpha,e)+A(a,e,i)$	same as (1)	same as (1)	$\frac{1}{2\pi}\sqrt{\frac{a}{\mu}}\left[f_{12}\frac{\sqrt{1-e^2}}{e}(-2\sigma\, e\sin\alpha - 3\alpha + \cos\alpha\sin\alpha) + f_3\cot i\sin\omega\;G(\sigma,\alpha,e)\right] + A(a,e,i)$
$\frac{d\Delta\tilde{V}}{dt}$	$\frac{1}{\pi}\sqrt{(f_{12})^2+(f_3)^2}\,(\alpha+\sigma\, e\sin\alpha)$	same as (1)	same as (1)	same as (1)

Apogee burns have $\sigma=+1$, perigee burns have $\sigma=-1$.

$$G(\sigma,\alpha,e)\equiv\frac{2\sigma\sin\alpha\,(1+e^2)+3e\alpha+e\cos\alpha\sin\alpha}{\sqrt{1-e^2}},\quad H(\sigma=-1,\alpha)\equiv\int_0^{\alpha}\frac{\cos E\,(1-e\cos E)}{\sqrt{1-e^2\cos^2 E}}dE,\quad H(\sigma=+1,\alpha)\equiv\int_{\pi}^{\pi+\alpha}\frac{\cos E\,(1-e\cos E)}{\sqrt{1-e^2\cos^2 E}}dE$$

Nodal regression rate: $N(a,e,i)\equiv\frac{-3}{2}\sqrt{\frac{\mu}{a^3}}\,J_2\left(\frac{R_e}{a}\right)^2\frac{\cos i}{\left(1-e^2\right)^2}$. Apsidal rotation rate: $A(a,e,i)\equiv\frac{3}{4}\sqrt{\frac{\mu}{a^3}}\,J_2\left(\frac{R_e}{a}\right)^2\frac{4-5\sin^2 i}{\left(1-e^2\right)^2}$

efficiently change e while keeping a constant. Case (4) has the in-plane acceleration parallel to the major axis of the ellipse, which gives no change in a, e, i, or Ω, but (unlike the other in-plane cases) does produce a change in ω. The formula in Table 3 for the buildup rate of ΔV is derived from the burn duration per revolution,

$$t_{burn} = 2\sqrt{a^3/\mu}\,(\alpha + \sigma\, e \sin\alpha), \qquad (3)$$

where the parameter σ equals -1 for perigee burns and $+1$ for apogee burns.

Only the out-of-plane component of acceleration f_3 affects the orientation of the orbit plane, and hence the four in-plane steering cases give the same results for i and Ω in Table 3. The function $G(\sigma, \alpha, e)$ appears in the rates of change of i, Ω, and ω, and the graph of G in Fig. 4 shows that apogee burns are much more effective than perigee burns for adjusting these elements. This graph also indicates that plane changing at a fixed yaw angle is inefficient when the apogee burn arc extends over more than half of the ellipse ($\alpha > \pi/2$). A maneuver to change i is best performed with $\omega = 0$ or π, because the rate of change of i is proportional to cos ω. Similarly, a maneuver to change Ω is best performed with $\omega = \pi/2$ or $3\pi/2$. Due to the i-dependence of the formulas in Table 3, the rates of change of Ω and ω become infinite as the inclination approaches zero, but the rate of change of the longitude of periapsis ($\Pi \equiv \Omega + \omega$) remains finite.

Earth's oblateness has a perturbing influence on Ω and ω that is expressed in Table 3 by the formulas for the nodal regression rate $N(a, e, i)$ and apsidal rotation rate $A(a, e, i)$;[8] these are added to the secular rates of change of Ω and ω due to thrusting. Apsidal rotation is a concern for elliptical orbit transfers that involve plane changing, because ω tends to drift away from the optimal value (e.g., $\omega = 0$ for a Δi maneuver). The examples in this paper take account of Earth's oblateness, but ignore other perturbations such as lunar-solar gravitation and solar radiation pressure.[5] The effects of satellite eclipsing and variable acceleration are also neglected.

Applications

The first application we will consider is a co-planar transfer between orbits of different eccentricities, which yields simple analytic expressions for the velocity increment and trip time. The mission is performed using inertially fixed steering with the acceleration perpendicular to the major axis of the ellipse, namely case (3) steering with $\alpha = \pi$. The semimajor axis a is unchanged during the maneuver, and from Table 3 the secular rate of e and the ΔV are

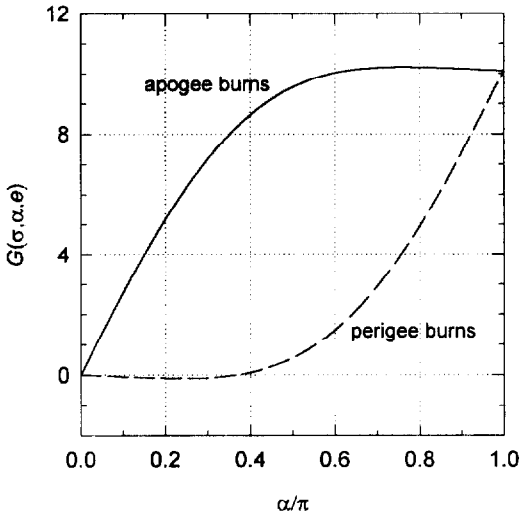

Figure 4. Dependence of the function G on α, as defined in Table 3. Orbit parameters are the same as in Fig. 3. Secular rates of change of i, Ω, and ω are proportional to G.

$$\left|\frac{de}{dt}\right| = \frac{3}{2} f \sqrt{\frac{a}{\mu}}\sqrt{1-e^2}\,, \qquad (4)$$

$$\Delta V = f\,\Delta t = \frac{2}{3}\sqrt{\frac{\mu}{a}}\,\left|\arcsin e_1 - \arcsin e_2\right|. \qquad (5)$$

Circularizing a 24-hour orbit with an initial apogee radius of 67,000 km (e = 0.58903) gives ΔV = 1.291 km/s with Δt = 50 days at an acceleration of $f = 3\times10^{-7}$ km/s^2. This describes the low-thrust portion of the geosynchronous equatorial orbit (GEO) insertion proposed by Spitzer[9] using a combination of chemical and electric propulsion. An acceleration of 3×10^{-7} km/s^2 corresponds to a thruster producing 50 mN per kW of input power and a satellite having a power-to-mass ratio of 6 W/kg.[7] Inertially fixed steering is chosen mainly for ease of implementation on geosynchronous satellites, but it happens to give a ΔV only a few percent greater than that of an optimized steering program. To illustrate this, compare Eq. (5) in the limit of small e with Edelbaum's result for changing the eccentricity of a near-circular orbit:[10]

$$\text{Inertially fixed:} \quad \Delta V = 0.667\sqrt{\mu/a}\,\Delta e\,, \qquad (6)$$

$$\text{Edelbaum optimal:} \quad \Delta V = 0.649\sqrt{\mu/a}\,\Delta e\,. \qquad (7)$$

The next application is a co-planar transfer from a circular low-earth orbit (LEO) to a 12-hour Molniya orbit (a = 26,554 km, e = 0.7) that allows viewing the high-latitude regions of the earth from an inclination of $i = 63.44°$ where the apsidal rotation rate is zero. Figure 5 shows the history of a and e for a transfer using perigee burns and case (2) steering with

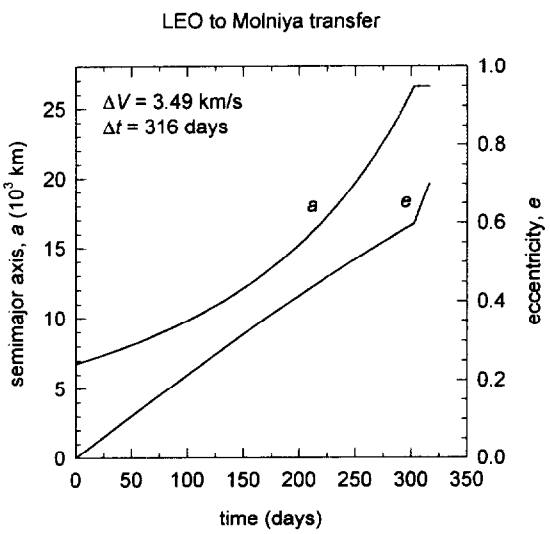

Figure 5. Semimajor axis and eccentricity vs. time for a co-planar LEO-to-Molniya transfer with $f = 3 \times 10^{-7}$ km/s^2 using perigee burns, case (2) steering, and $\alpha = \pi/2$.

$\alpha = \pi/2$, corresponding to tangential thrusting along half of the ellipse. The first part of the transfer ends at 303 days, when a = 26,554 km and e = 0.5976. The maneuver technique then changes to case (3) steering with continuous thrusting perpendicular to the major axis, which brings e to the desired value in 13 days while a remains constant. Because the first segment of this mission uses perigee-centered burns, the ΔV and trip time are less for case (2) steering (3.49 km/s, 316 days) than for case (1) steering (3.79 km/s, 331 days). A reduction in trip time to 224 days and an increase in ΔV to 5.79 km/s are attained by thrusting continuously ($\alpha = \pi$) to reach a circular orbit at a = 26,554 km, followed by a maneuver to change from e = 0 to e = 0.7. Alternatively, if the burn arc is reduced by choosing $\alpha = 55°$ then both a and e reach their target values after 520 days with a greatly reduced ΔV of 2.75 km/s. However, these results all imply that low-thrust propulsion is not a very attractive option for transfers to highly eccentric orbits.

As an example of an elliptical orbit transfer with a plane change, we consider moving to GEO from an orbit having an apogee altitude of 35,786 km, a perigee altitude of 185 km, and $i = 28.5°$. This requires increasing the semimajor axis while bringing the eccentricity and inclination to zero. Figure 6 shows the history of the orbital elements for a transfer using apogee burns with case (1) steering, a burn arc of $\alpha = \pi/2$ (i.e., half of the ellipse), and a yaw angle held constant at $\beta = 42.2°$. The latter is chosen to make a and i reach their target values at the same time (117 days), from which point the orbit is circularized using case (3) steering with continuous in-plane acceleration

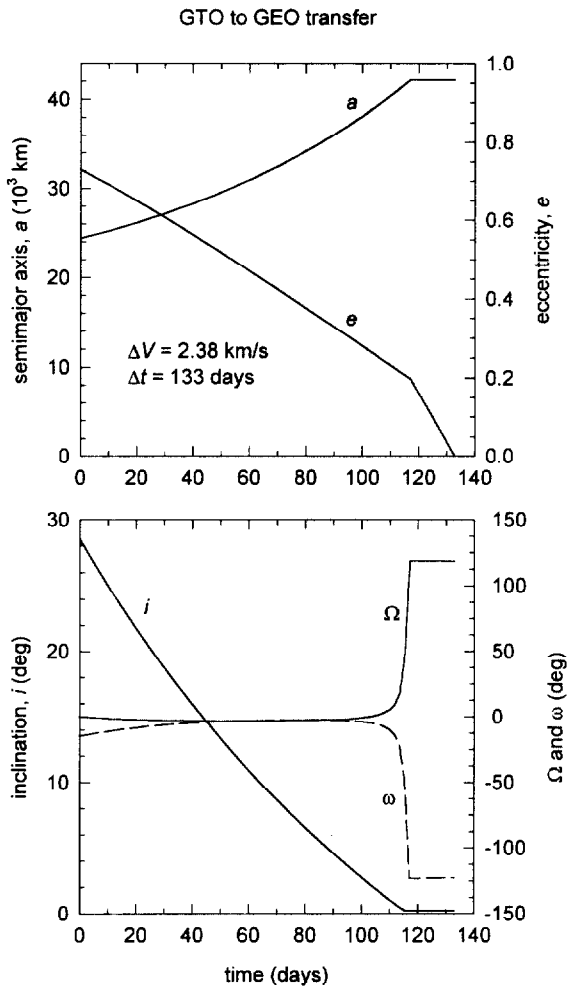

Figure 6. Orbital elements vs. time for a GTO-to-GEO transfer with $f = 3 \times 10^{-7}$ km/s^2 using apogee burns, case (1) steering, $\alpha = \pi/2$, and a constant yaw angle of $\beta = 42.2°$.

perpendicular to the major axis. To get around the problem of apsidal rotation, the argument of perigee is initialized at $\omega = -15°$ and drifts naturally toward $\omega = 0°$ as i approaches zero. The total ΔV is 2.38 km/s for the low-thrust mission with $\alpha = \pi/2$, compared with an impulsive (high thrust) ΔV of 1.84 km/s. Using $\alpha > \pi/2$ shortens the trip time slightly but incurs a large ΔV penalty, while using $\alpha < \pi/2$ gives a modest ΔV savings at the cost of a much longer trip time.

To illustrate how our method can assist in top-level trade studies, we consider a transfer to GEO for a range of initial conditions. In this scenario the launch vehicle initially places the satellite in an orbit with a variable apogee radius, a perigee at LEO, and $i = 28.5°$. The on-board chemical system then fires at apogee to reach a park orbit having a perigee radius of 15,000 km and a variable inclination. This perigee radius is

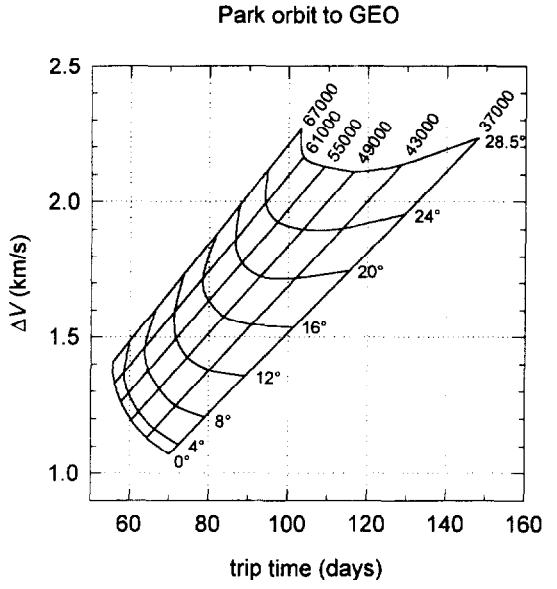

Figure 7. Velocity increment vs. trip time to reach geosynchronous equatorial orbit from a park orbit with a perigee radius of 15,000 km. Park apogee radius (km) and inclination (°) are specified on the graph.

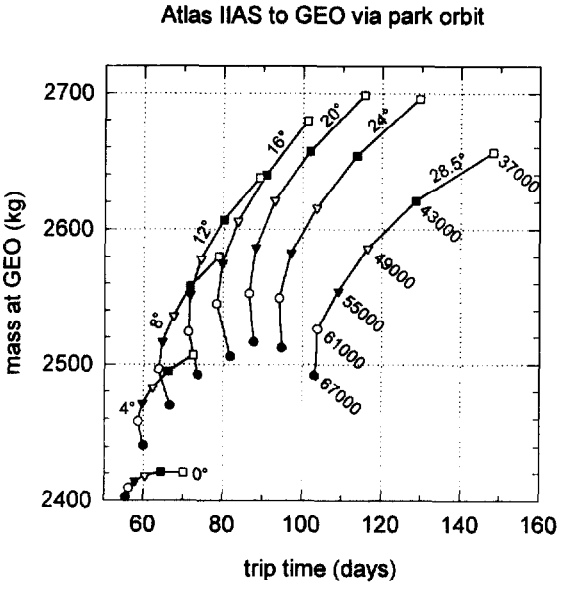

Figure 8. Satellite mass vs. trip time to reach geosynchronous equatorial orbit from an Atlas IIAS booster via a park orbit with a perigee radius of 15,000 km. Park apogee radius (km) and inclination (°) are specified on the graph.

selected to minimize exposure to high-energy protons during the low-thrust segment of the mission. The spacecraft travels to GEO by the same approach as in Fig. 6 at an acceleration of $f = 3\times10^{-7}$ km/s^2, with the yaw angle β and the initial ω chosen to give $i = 0°$ when $a = 42{,}164$ km. Figure 7 shows ΔV as a function of trip time for the low-thrust maneuver with the park apogee and inclination displayed parametrically. For a given apogee radius, there is a linear relation between ΔV and trip time, governed by the choice of park inclination (more Δi means a longer trip and greater ΔV). For a given park inclination, ΔV can be either a decreasing or increasing function of trip time depending on park apogee radius. It is perhaps surprising to see for $i \leq 16°$ that the ΔV to GEO *increases* as the park apogee radius increases. This comes about because the park orbit eccentricity increases with apogee radius, and the higher ΔV for circularization more than offsets the lower ΔV needed to change a. A different trend can be seen for $i > 16°$ when an intermediate apogee radius (ca. 49,000 km) gives the minimum ΔV, due to the penalty associated with plane changing at lower radii.

Typically the mission planner seeks to maximize payload mass at GEO for a given trip time, which is not necessarily achieved by minimizing the low-thrust ΔV. With a given launch vehicle, the attainable spacecraft mass in the park orbit depends on apogee radius and inclination (i.e., decreased mass if the orbit is higher and less inclined). Hence, the results in Fig. 7 must be combined with performance figures for the launch vehicle and on-board chemical system to optimize the mass-vs-time trade-off to GEO. This is depicted in Fig. 8 for the case of an Atlas IIAS booster with the park perigee radius fixed at 15,000 km. On-board propulsion systems are assumed to have specific impulses of 314 s (chemical) and 1600 s (electric). Several interesting trends are evident in Fig. 8. If the park orbit is confined to $i = 0°$ (equatorial), then the best apogee radius is around 50,000 km, and the satellite mass at GEO is 2420 kg with a 60-day trip time (an improvement of at least 400 kg over an all-chemical propulsion system). Further mass gains are possible if the spacecraft can perform yaw steering to change inclination during the low-thrust segment of the mission. A satellite mass of 2610 kg and an 80-day trip time are achieved when the park orbit inclination is $i = 12°$ and the apogee radius is 43,000 km. No additional benefit is obtained for park orbit inclinations greater than $i = 20°$. Similarly, apogee radii greater than 55,000 km are to be avoided, because they give a sharp reduction in GEO mass with little or no savings in trip time. One exception to this would be for an equatorial park orbit ($i = 0°$) with a 24-hour period (e.g., 69,328-km apogee radius, 15,000-km perigee radius) that is circularized with inertially fixed steering while in view of a single ground station.[9] Here the mission planner may decide that operational simplicity is of greater value than incremental gains in mass and trip time.

Acknowledgement

This work is supported by the Internal Research and Development Program at the Aerospace Corporation.

References

1. K.P. Zondervan, et al. "Guidance, navigation, and control trades for an electric orbital transfer vehicle," Paper AIAA-90-3458-CP, Guidance, Navigation, and Control Conference, 20-22 Aug 1990, Portland, Oregon; and Aerospace Report No. TOR-93(3514)-1, (Dec 1992).

2. C.E. Vaughan and R.J. Cassady, "An updated assessment of electric propulsion technology for near-Earth space missions," Paper AIAA-92-3202, 28th Joint Propulsion Conference, 6-8 July 1992, Nashville, TN.

3. F. Porte, et al. "Application of ion propulsion system to communications spacecraft," Paper IEPC-93-015, 23rd International Electric Propulsion Conference, 13-16 Sept 1993, Seattle, WA.

4. S.R. Oleson and R.M. Myers, "Launch vehicle and power level impacts on electric GEO insertion," Paper AIAA-96-2978, 32nd Joint Propulsion Conference, 1-3 July 1996, Lake Buena Vista, FL.

5. A.G. Schwer and E. Messerschmid, "System and mission optimization of geostationary telecommunication satellites using arcjet propulsion systems," Paper AIAA-97-2713, 33rd Joint Propulsion Conference, 6-9 July 1996, Seattle, WA.

6. E.G.C. Burt, "On space manoeuvres with continuous thrust," Planet. Space Sci. 15, 103-122 (1967).

7. J.E. Pollard and S.W. Janson, "Spacecraft electric propulsion applications," ATR-96(8201)-1, The Aerospace Corporation (1 Feb 1996).

8. M.D. Griffin and J.R. French, Space Vehicle Design, (American Institute of Aeronautics and Astronautics, Washington, DC, 1991).

9. A. Spitzer, "Near optimal transfer orbit trajectory using electric propulsion," Paper AAS-95-215, Spaceflight Mechanics Meeting, 13-16 Feb 1995, Albuquerque, NM.

7. T.N. Edelbaum, "Propulsion requirements for controllable satellites," ARS Journal, 31, 1079 (1961).